



Temporal controls on global dust emissions: The role of surface gustiness

S. Engelstaedter¹ and R. Washington¹

Received 9 March 2007; revised 12 May 2007; accepted 5 July 2007; published 7 August 2007.

[1] Topographic depressions serve as the key spatial control on large global dust sources. In contrast, the temporal control on these hotspots has remained elusive. We provide the first global observational evidence that the annual cycle of emissions from dust hotspots is determined by an erosivity feature in the form of wind gustiness. We use TOMS AI and an aridity index to define 131 global dust hotspots. The correlation between the annual cycle of hotspot dust and the annual cycle of gustiness is 70% stronger than the corresponding correlation with wind. The mean significant correlation with wind ($n = 106$ hotspots) is 0.37 ($\sigma = 0.24$) and the mean of significant correlation ($n = 118$ hotspots) with gustiness is 0.63 ($\sigma = 0.12$). Whereas most model simulations of dust have relied on the broadscale wind, gustiness holds overwhelmingly more power in explaining the annual cycle of dust emissions from global dust hotspots. **Citation:** Engelstaedter, S., and R. Washington (2007), Temporal controls on global dust emissions: The role of surface gustiness, *Geophys. Res. Lett.*, 34, L15805, doi:10.1029/2007GL029971.

1. Introduction

[2] Mineral dust is known to alter climate by changing the Earth's radiation budget [Haywood *et al.*, 2001; Sokolik *et al.*, 2001; Tegen *et al.*, 1996], and influencing biogeochemical cycles [Jickells *et al.*, 2005; Kaufman *et al.*, 2005; Swap *et al.*, 1992; Talbot *et al.*, 1986] and cloud characteristics [Rosenfeld *et al.*, 2001]. Dust also has an impact on human health [Prospero, 1999; Sultan *et al.*, 2005]. Owing to its impact on the Earth's energy budget, the inclusion of dust in climate models is clearly vital for the realistic simulation of past, present and future climates. If dust emission is not well simulated, all subsequent processes involving dust in the atmosphere will not be realistic either. While climatically important atmospheric gases such as CO₂ are well mixed in the atmosphere, constituents like mineral dust, which account for about 75% of the global aerosol mass load and 25% of the global aerosol optical depth [Kinne *et al.*, 2006], have a short residence time, seldom longer than two weeks. Representing the dust cycle in modeling efforts therefore requires precise spatial and temporal simulation of dust emissions so that the impacts of dust on climate can be treated in realistic locations and at appropriate times in the annual cycle.

[3] Recent progress with constraining dust emissions spatially came with the 'preferred source' concept following

analysis of the first available long term mean satellite aerosol product Total Ozone Mapping Spectrometer absorbing Aerosol Index (TOMS AI) [Herman *et al.*, 1997; Prospero *et al.*, 2002; Washington *et al.*, 2003]. Based on the observation that peaks in the spatial distribution of the long-term mean TOMS AI coincide with the geographic distribution of topographic depressions, it has been argued that increased sediment accumulation characterizes the depressions [Washington *et al.*, 2006]. These sediments are often the relicts of now desiccated Holocene lakes, which have an increased potential for deflation given a low or non-existent vegetation cover. Dust models, adopting preferred source regions on the basis of topographic depressions in regions with low vegetation, showed a greatly improved simulation of atmospheric dust loadings and transport [Ginoux *et al.*, 2001; Tegen *et al.*, 2002; Zender *et al.*, 2003]. The temporal controls on variability, particularly in hyper arid locations where the majority of mineral dust originates, have in contrast remained poorly understood.

[4] Dust emission occurs when wind stress acting on soil particles exceeds a threshold [Gillette, 1974], a process which mainly depends on surface roughness, particle size, soil moisture and wind characteristics. Although changes in soil moisture and vegetation cover affect the annual cycle of dust emission in some deserts, changes in the surface winds are the more important control on emissions in hyper-arid deserts which dominate dust production [Prospero *et al.*, 2002] and where vegetation cover does not change significantly over the year.

[5] In most climate models, wind speed is given as an instantaneous value for a specific model integration time-step averaged in space over the area of a grid box. Therefore, wind speed represents the broadscale wind at a given time. In contrast, a wind gust is a sudden brief increase in wind speed, generally less than 20 s, which in most climate models is a parameterized semi-instantaneous value (e.g. for ERA-40 it is the maximum gust within the previous 3 hours) averaged over the grid box area. Therefore, gustiness here represents a measure of the magnitude of short-lived high wind events which can also be taken as an indicator of wind variability. In this study we test the hypothesis that on a global scale wind gusts exert a stronger temporal control on the annual cycle of dust emission from desert environments than the broadscale winds.

2. Approach and Methodology

2.1. Specification of Source Regions

[6] In order to evaluate the temporal controls on dust emission, we start by identifying sources of dust emission in the Earth's deserts and drylands using the TOMS AI [Herman *et al.*, 1997]. The satellite derived index which is

¹Climate Research Laboratory, Centre for the Environment, University of Oxford, Oxford, U. K.

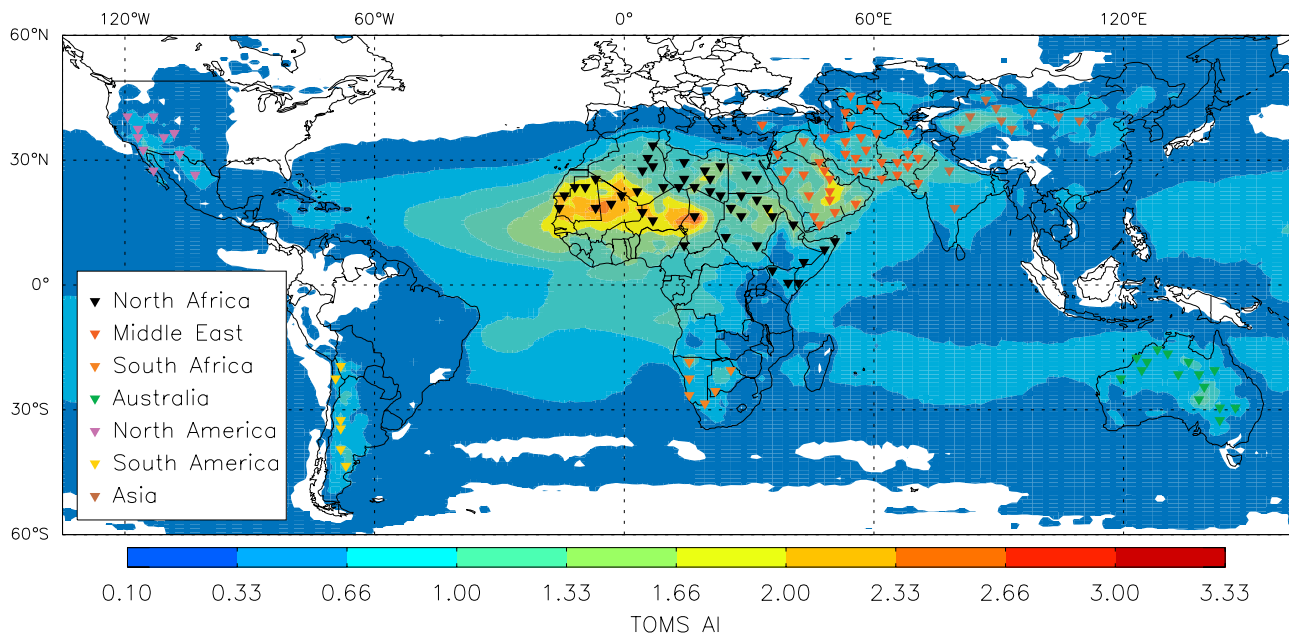


Figure 1. Long-term mean TOMS AI averaged over 1984–1990 and location of 131 dust hot spots with coded regional designation.

based on the spectral difference between two UV channels (340 nm and 380 nm) for the Nimbus 7 satellite which flew from November 1978 to May 1993, can be used as an indicator for the amount of dust suspended in the atmosphere. Although it has been suggested that the applied algorithm may not be able to detect dust at low levels close to the ground [Herman *et al.*, 1997], it provides one of the longest continuous records. We here use TOMS AI data version 8 available on a 1.25° longitude by 1° latitude grid from January 1984 to December 1990 when the TOMS AI was most stable and not affected by volcanic aerosols.

[7] Assuming that highest values in the TOMS AI occur close to the source regions, a hotspot is defined as a grid box where the long-term mean TOMS AI is greater than or equal to 0.5 and higher than that of any of the 8 surrounding grid boxes. We only include hotspots in regions classified by the *United Nations Environmental Programme* [1992] as hyper-arid, arid and semi-arid based on an aridity index of annual precipitation over potential evapotranspiration available at 1° resolution. This results in the exclusion of some falsely identified dust hotspots because of the TOMS AI's sensitivity to biomass burning aerosols. One hotspot was excluded as the TOMS AI annual dust cycle calculated for subsequent analysis had missing values. The application of this algorithm results in the identification of 131 dust hotspots (Figure 1).

2.2. Deriving the Annual Cycle of Dust and Winds

[8] Surface wind gustiness parameters were derived from the European Centre for Medium-Range Weather Forecasts (ECMWF) 40 year Re-Analysis (ERA-40) fields of 10 m surface wind speed and 10 m surface gustiness interpolated to local noon (to match the TOMS AI sampling time) for 1984 to 1990. The temporal interpolation to local noon was achieved as the weighted mean of the two corresponding grid boxes in the two ERA-40 files which temporally cover local noon at the specific longitude, with weights determined by the distance of the grid box from the two

respective longitudes represented by the time (UTC) of the ERA-40 files. In ERA-40, surface gustiness is a parameterized field which is thought to be comparable with gustiness measurements defined by the World Meteorological Organization (WMO) as the maximum wind averaged over 3 second intervals. The gustiness field is available as a 6-hour model forecast field since wind departing from the broad-scale flow is generally excluded in the assimilation process. Both wind datasets were regridded to 1.25° longitude by 1° latitude in order to match the TOMS AI spatial resolution.

[9] For each grid box identified as a dust hotspot (Figure 1), the annual cycles of TOMS AI, surface wind speed and surface gustiness were computed from the long-term mean between January 1984 and December 1990 from the first to the fifteenth day of each month and from the sixteenth to last day of each month ($n = 24$). Spearman's rank correlation coefficients are calculated between the annual cycle of TOMS AI and the annual cycle of surface wind speed and gustiness.

3. TOMS AI Correlations With Wind and Gustiness

[10] We identify 131 hotspots of dust emission using the method described in the previous section (Figure 1). Most of the identified hotspots are located in areas known to be dust source regions [see Goudie and Middleton, 2006, and references therein], and many coincide with point sources (e.g. playas, dry lakes or wadis) as described in the literature [e.g., Prospero *et al.*, 2002; Washington *et al.*, 2003]. Dust hotspots are found on all continents except Antarctica. With 78% ($n = 102$ hotspots) of the identified dust hotspots north of the equator, emissions predominate in the northern hemisphere between the equator and about 45°N , including desert regions of North America, North Africa, the Middle East and Asia. The other 22% ($n = 29$ hotspots) are located

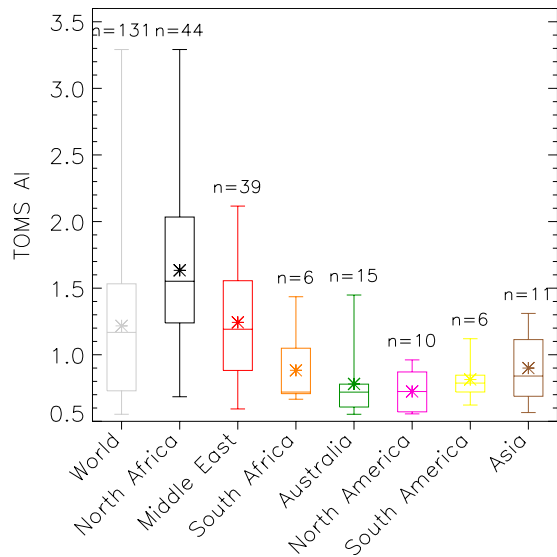


Figure 2. Long-term mean TOMS AI values and their variability derived from 131 dust hotspots as defined in Figure 1 for specific geographic regions. The arithmetic mean is represented by the asterisk. The horizontal line through the box represents the median, the lower edge of the box the 25%-percentile and the upper edge the 75%-percentile. The horizontal lines below and above the box represent the minimum and maximum value. The number of hot spots is given above each box.

in the southern hemisphere in dry regions of South America, southern Africa and Australia between 15°S and 45°S. The global average (arithmetic mean) TOMS AI for the hotspots is 1.22 with a maximum of 3.29 (Figure 2). Highest average emissions occur in North Africa (1.63) followed by the Middle East (1.24). Lower average emissions occur in Asia (0.9), South Africa (0.88), South America (0.81) and Australia (0.78), and lowest emissions occur in North America (0.72).

[11] For each of the 131 dust hotspots, we calculate the correlation between the annual cycle of dust and a) the annual cycle of wind speed ($r_{s,wind}$) and b) the annual cycle of surface gustiness ($r_{s,gust}$) in order to compare the control of these erosivity proxies on the timing of dust emissions (Figure 3).

[12] Surface gustiness dominates over surface winds in the correlation with dust over the annual cycle such that 88 of the 101 (or 87%) statistically significant ($p = 0.05$) dust hot spots show a stronger correlation between gustiness and TOMS AI than between wind speed and TOMS AI (Figure 3). The mean of significant $r_{s,wind}$ correlations ($n = 106$ hotspots) is 0.37 ($\sigma = 0.24$) and the mean of significant $r_{s,gust}$ correlations ($n = 118$ hotspots) is 0.63 ($\sigma = 0.12$). This represents an increase in the mean correlation coefficients of 70%.

[13] Both $r_{s,wind}$ and $r_{s,gust}$ show some negative correlations, 25 and 6 significant negative correlations respectively. At 14 of 25 dust hot spots with significant negative correlation for $r_{s,wind}$ there were significant positive correlation for $r_{s,gust}$ whereas no negative correlation for $r_{s,gust}$ matched positive correlations for $r_{s,wind}$ showing the clear improvement of gustiness in explaining the timing of dust emissions. There is little bias to the geographical location of

the correlations where gustiness performs better than surface wind suggesting that the control exerted by gustiness in the annual cycle can be considered to be global.

[14] The key result in this paper is insensitive to the specification of a TOMS AI threshold of 0.5 in the hotspot definition. Relaxing the TOMS AI threshold to 0.1 produces 182 hotspots with mean significant correlation coefficients of 0.36 and 0.61 for $r_{s,wind}$ and $r_{s,gust}$ respectively. Increasing the threshold to 1.0 produces 72 hotspots with mean significant correlation coefficients of 0.48 and 0.67 for $r_{s,wind}$ and $r_{s,gust}$ respectively. In both cases, gustiness outperforms the broadscale wind in explaining the annual cycle of dustiness and does so with very similar proportional success as reported for the 131 hotspots obtained with an AI of 0.5. The TOMS AI threshold of 0.5 was chosen as it yields a large sample of global dust hotspots without

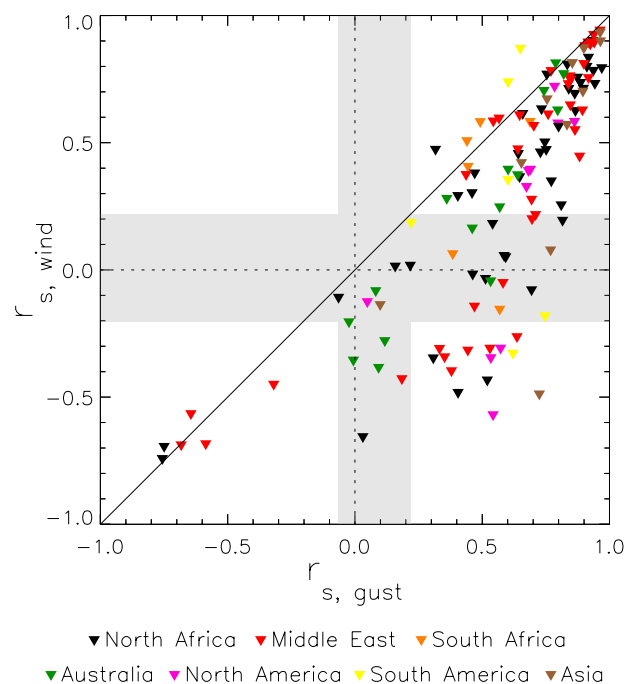


Figure 3. Spearman's rank correlation coefficient scatter plot for the annual cycle of TOMS AI and 10 m surface wind speed ($r_{s,wind}$) versus the annual cycle of TOMS AI and surface wind gusts ($r_{s,gust}$) for 131 global dust hot spots (triangles; symbols in b/w version). The annual cycle used for the calculations yields 24 values, two averages per month (1st to 15th day and 16th to last day of the month), and are calculated over the period January 1984 to December 1990. Insignificant correlation coefficients are marked for $r_{s,wind}$ and $r_{s,gust}$ by a horizontal and vertical gray bar respectively. The geographical region of the dust hot spots is indicated by the color of the triangles (by the symbol in b/w version). The diagonal solid black line from the lower left corner of the plot to the upper right corner defines where both $r_{s,wind}$ and $r_{s,gust}$ are equal. The area left of that line indicates where correlation coefficients between wind speed and TOMS AI ($r_{s,wind}$) are stronger than between gustiness and TOMS AI ($r_{s,gust}$). The area right of that line indicates where gustiness and TOMS AI ($r_{s,gust}$) shows a stronger correlation than wind speed and TOMS AI ($r_{s,wind}$).

including unrealistic sources which are the result of TOMS AI's background noise and biomass burning sensitivity.

[15] These statistics show that on a global scale the annual cycle of TOMS AI relates better to the annual cycle of surface gustiness than surface wind speed. Sub-grid scale wind variability is clearly an important erosivity factor for the emission of dust from deserts and drylands on a global scale.

4. Discussion

[16] The improvement of wind gustiness over the broad-scale wind in explaining the timing of dust emission can be traced to two possible causes: a) differences in the way that the ECMWF model corrects the broadscale wind values to low roughness settings compared with the (uncorrected) gustiness and b) the parameterization of wind variability.

[17] We consider the difference between the correction of the broadscale wind and gustiness by surface roughness in ERA-40 next. In order to make ERA-40 wind fields comparable with the standard level of 10 m for surface synoptic observations (SYNOP), 10 m surface wind speed is computed by vertical interpolation between the lowest model level and the surface [ECMWF, 2001]. As the WMO requires SYNOP stations to be located in open terrain in order to be well exposed to wind, the ERA-40 10 m surface wind field is computed using the concept of exposure correction whereby the surface roughness length has a value of 0.03 m (representing grassland) for all grid boxes where roughness is greater than 0.03 m. For dust models which use the ERA-40 10 m surface wind field to calculate emissions, the exposure correction introduces a potential error as the wind speed and variability may not accurately represent real-world conditions in some regions where the roughness is an important factor in determining those wind characteristics.

[18] The 10 m surface gustiness field is intended to be comparable to WMO observations and is computed as a function of horizontal wind variability including the effects of surface friction (through surface roughness) and atmospheric stability [ECMWF, 2001]. However, the wind variability used to estimate gustiness is based on 10 m surface wind speeds computed without exposure correction. Therefore, wind variability here is likely to be higher over inhomogeneous terrain compared to the 10 m surface wind field computed including the exposure correction. The observed difference in the relationship between the annual cycle of TOMS AI and wind ($r_{s,wind}$) and TOMS AI and gustiness ($r_{s,gust}$) (Figure 3) may therefore result from the different ways in which surface winds are computed for the 10 m surface wind speed field (exposure correction) and 10 m surface gustiness field (no exposure correction).

[19] This is, however, not the case. About a third ($n = 40$) of the 131 dust hotspots are located in regions where the surface roughness length is less than 0.03 m. Therefore these hotspots are not affected by the exposure correction. Some 93% ($n = 27$) of the significant correlations ($n = 29$) of these hotspots show a significant increase in the correlation between gustiness and dust compared to surface wind speed and dust which is in the same order of magnitude as for the whole 131 dust hotspots (not shown). Therefore, we are confident that that the relationship presented in Figure 3 indeed reflects the difference between the broadscale wind

and gustiness rather than the difference in the computation of the respective ERA-40 10 m surface wind speed field.

[20] A key explanation for the enhanced explanatory power of gustiness must therefore rest with the way ERA-40 parameterizes surface gustiness, assuming that ERA-40 does not simulate the gustiness events which actually occur in the real world. Wind observations used in the assimilation process are extremely sparsely distributed in the regions of almost all of the 131 dust hotspots and the gustiness component in the observed wind field, where such data are present, is invariably excluded during assimilation. From this perspective it is very surprising that gustiness performs so much better than the mean wind, particularly given the cubic dependence of emissions on surface wind speed which acts to amplify any errors resulting from a parameterization process. Dust emission has nevertheless been shown to occur as a result of scales well below that of climate models [Koch and Renno, 2005]. The suggestion here is that the gustiness parameterization represents wind characteristics which are closer to these smaller scales and are capable of being representative even in coarse spatial scale models. The results here strongly suggest that the use of the gustiness parameter as a driver of emissions in dust models may well improve model performance.

5. Summary

[21] Using the satellite derived TOMS AI and ECMWF ERA-40 reanalysis fields of 10 m surface wind speed and 10 m surface gustiness, we show that for 131 global dust hotspots identified from the long-term mean TOMS AI, surface gustiness exerts a much stronger temporal control on the timing of emissions than the broadscale winds. The results highlight the importance of localized high wind events such as gusts as a driver of dust emissions from the Earth's deserts.

[22] Long-term measurements of high resolution wind characteristics and atmospheric dust in source regions are needed to verify and quantify the observed relationship between dust emission and gustiness on the ground. A future study will look into the possibility of whether the ECMWF ERA-40 gustiness parameter can be implemented in global dust models and whether this will improve model simulations of the global dust cycle.

[23] **Acknowledgment.** We would like to thank N. Mahowald and T. E. Gill for helpful comments.

References

- European Centre for Medium-Range Weather Forecasts (ECMWF) (2001), *IFS Documentation Cycle CY23r4, Part IV: Physical Processes (CY23R4)*, edited by P. White, 144 pp., Reading, U. K. (Available from http://www.ecmwf.int/research/ifsdocs_old/PHYSICS/index.html.)
- Gillette, D. A. (1974), On the production of soil wind erosion aerosols having the potential for long range transport, *J. Rech. Atmos.*, *8*, 735–744.
- Ginoux, P., M. Chin, I. Tegen, J. M. Prospero, B. Holben, O. Dubovik, and S. J. Lin (2001), Sources and distributions of dust aerosols simulated with the GOCART model, *J. Geophys. Res.*, *106*, 20,255–20,273.
- Goudie, A. S., and N. J. Middleton (2006), *Desert Dust in the Global System*, Springer, New York.
- Haywood, J. M., P. N. Francis, M. D. Glew, and J. P. Taylor (2001), Optical properties and direct radiative effect of Saharan dust: A case study of two Saharan dust outbreaks using aircraft data, *J. Geophys. Res.*, *106*, 18,417–18,430.
- Herman, J. R., P. K. Bhartia, O. Torres, C. Hsu, C. Seftor, and E. Celarier (1997), Global distribution of UV-absorbing aerosols from Nimbus 7/TOMS data, *J. Geophys. Res.*, *102*, 16,911–16,922.

- Jickells, T. D., et al. (2005), Global iron connections between desert dust, ocean biogeochemistry, and climate, *Science*, *308*, 67–71.
- Kaufman, Y. J., I. Koren, L. A. Remer, D. Tanre, P. Ginoux, and S. Fan (2005), Dust transport and deposition observed from the Terra-Moderate Resolution Imaging Spectroradiometer (MODIS) spacecraft over the Atlantic Ocean, *J. Geophys. Res.*, *110*, D10S12, doi:10.1029/2003JD004436.
- Kinne, S., et al. (2006), An AeroCom initial assessment: Optical properties in aerosol component modules of global models, *Atmos. Chem. Phys.*, *6*, 1815–1834.
- Koch, J., and N. O. Renno (2005), The role of convective plumes and vortices on the global aerosol budget, *Geophys. Res. Lett.*, *32*, L18806, doi:10.1029/2005GL023420.
- Prospero, J. M. (1999), Long-term measurements of the transport of African mineral dust to the southeastern United States: Implications for regional air quality, *J. Geophys. Res.*, *104*, 15,917–15,927.
- Prospero, J. M., P. Ginoux, O. Torres, S. E. Nicholson, and T. E. Gill (2002), Environmental characterization of global sources of atmospheric soil dust identified with the NIMBUS 7 Total Ozone Mapping Spectrometer (TOMS) absorbing aerosol product, *Rev. Geophys.*, *40*(1), 1002, doi:10.1029/2000RG000095.
- Rosenfeld, D., Y. Rudich, and R. Lahav (2001), Desert dust suppressing precipitation: A possible desertification feedback loop, *Proc. Natl. Acad. Sci. U. S. A.*, *98*, 5975–5980.
- Sokolik, I. N., D. M. Winker, G. Bergametti, D. A. Gillette, G. Carmichael, Y. J. Kaufman, L. Gomes, L. Schuetz, and J. E. Penner (2001), Introduction to special section: Outstanding problems in quantifying the radiative impacts of mineral dust, *J. Geophys. Res.*, *106*, 18,015–18,027.
- Sultan, B., K. Labadi, J. F. Guegan, and S. Janicot (2005), Climate drives the meningitis epidemics onset in West Africa, *PLoS Medicine*, *2*, 43–49.
- Swap, R., M. Garstang, S. Greco, R. Talbot, and P. Kallberg (1992), Saharan dust in the Amazon Basin, *Tellus, Ser. B*, *44*, 133–149.
- Talbot, R. W., R. C. Harriss, E. V. Browell, G. L. Gregory, D. I. Sebacher, and S. M. Beck (1986), Distribution and geochemistry of aerosols in the tropical North Atlantic troposphere: Relationship to Saharan dust, *J. Geophys. Res.*, *91*, 5173–5182.
- Tegen, I., A. A. Lacis, and I. Fung (1996), The influence on climate forcing of mineral aerosols from disturbed soils, *Nature*, *380*, 419–422.
- Tegen, I., S. P. Harrison, K. Kohfeld, I. C. Prentice, M. Coe, and M. Heimann (2002), Impact of vegetation and preferential source areas on global dust aerosol: Results from a model study, *J. Geophys. Res.*, *107*(D21), 4576, doi:10.1029/2001JD000963.
- United Nations Environmental Programme (1992), *World Atlas of Desertification*, Edward Arnold, Sevenoaks, U. K.
- Washington, R., M. Todd, N. J. Middleton, and A. S. Goudie (2003), Dust-storm source areas determined by the total ozone monitoring spectrometer and surface observations, *Ann. Assoc. Am. Geogr.*, *93*, 297–313.
- Washington, R., et al. (2006), Links between topography, wind, deflation, lakes and dust: The case of the Bodélé Depression, Chad, *Geophys. Res. Lett.*, *33*, L09401, doi:10.1029/2006GL025827.
- Zender, C. S., H. Bian, and D. Newman (2003), Mineral Dust Entrainment and Deposition (DEAD) model: Description and 1990s dust climatology, *J. Geophys. Res.*, *108*(D14), 4416, doi:10.1029/2002JD002775.

S. Engelstaedter and R. Washington, Climate Research Laboratory, Centre for the Environment, University of Oxford, South Parks Road, Oxford OX1 3QY, UK. (engelstaedter@ouce.ox.ac.uk)